VerJK21102023

Inactivation of Influenza virus as representative of enveloped RNA viruses on photocatalytically active nanoparticle and nanotubular TiO_2 surfaces

M. Baudys[a], H. Sopha[b,c], J. Hodek[d], J. Rusek[a], H. Bartková[a], L. Ulrychová[d,e], J. M. Macak[b,c], J. Weber[d], J. Krýsa[a*]

[a] Department of Inorganic Technology, University of Chemistry and Technology Prague, Technicka 5, 166 28 Prague, Czech Republic

[b] Center of Materials and Nanotechnologies, Faculty of Chemical Technology, University of Pardubice, Nam. Cs. Legii 565, 53002 Pardubice, Czech Republic

[c] Central European Institute of Technology, Brno University of Technology, Purkyňova 123, 612 00 Brno, Czech Republic

[d] Institute of Organic Chemistry and Biochemistry of the Czech Academy of Sciences, Flemingovo nám. 2, 166 10 Prague, Czech Republic

[e] Department of Genetics and Microbiology, Faculty of Sciences, Charles University, Viničná 5, 128 44 Prague, Czech Republic

Abstract

The recent pandemic showed us that there is a strong demand for standardized methods to evaluate the antiviral activity of different materials using enveloped RNA viruses (e.g. SARS-CoV-2, influenza virus). Virucidal activity can be achieved as a result of photoexcitation of TiO_2 photocatalyst under UV illumination. All standardized methods evaluating the virucidal activity of photocatalytic surfaces use bacteriophage Q-beta, a representative of small non-enveloped viruses. This work was thus devoted to the evaluation of the virucidal efficiency of photocatalytically active nanostructured TiO_2 surfaces (nanotubular and nanoparticle) to inactivate the influenza virus with particular interest to the methodology of virucidal testing and the influence of the surface nanostructure (porosity).

Two different TiO_2 nanostructures were used in this study, namely nanoparticle and nanotubular structures. A significant decrease in the amount of viral RNA and titer was obtained after the rinsing because the virus was retained on the surface of the nanostructured TiO_2 during exposure in the dark. The decrease can be understood as an additional effect of the surface porosity to the TiO_2 virucidal activity after UV illumination, however, this fact was taken into account in the calculation of virucidal activity due to UV light. Both nanostructured TiO_2 coatings have comparable porosity and thickness but the photocatalytic activity is higher for nanoparticle than for nanotubular surface. On the other hand, the virucidal activity is much higher for the nanotubular surface.

Keywords: TiO_2, photocatalysis, nanotubular layer, porosity, virucidal, Influenza virus.

* corresponding author

1. Introduction

Biocidal properties (e. g. antibacterial and virucidal activity) of surfaces are becoming very important due to their numerous applications as antibiofilm surfaces [1], antifouling surfaces [2] and surfaces suppressing the transmission of infectious diseases [3, 4]. Hybrid coatings and nanocomposites containing metallic nanoparticles, e.g. Ag, Cu, Zn, Au, Cu-Ti, etc. demonstrated antibacterial [5],[6] and virucidal [7],[8] properties (without UV irradiation). When a coating consists of titanium dioxide (TiO_2), antibacterial and virucidal activity can be achieved as a result of photoexcitation of the TiO_2 photocatalyst under UV illumination. This particular photoactivation of TiO_2 generates reactive oxygen molecules on the TiO_2 surface leading to the inactivation of bacteria and viruses.

Among various TiO_2 nanomaterials, the 1D nanotubular TiO_2 structures can be used in many applications due to their unique properties. Anodic oxidation of Ti substrates in a fluoride-containing electrolyte is the most often used technique to prepare TiO_2 nanotube layers [9, 10]. By adjusting the electrolyte composition, anodization potential and anodization time, the diameter and thickness of the resulting TiO_2 nanotube layers can be adjusted [11]. Compared to TiO_2 nanotubes prepared by other methods, resulting in TiO_2 nanotube powders, TiO_2 nanotubes prepared by anodization grow directly on the Ti foil in the form of vertically aligned nanotube layers with an open top and closed bottom, which adhere to the Ti substrate. No further immobilization of the TiO_2 nanotubes on a substrate using a binder is needed. Furthermore, due to the high order of the TiO_2 nanotube layers, they exhibit a straight diffusion path [12] [13].

The virucidal activity of TiO_2 coatings was investigated using various either unenveloped or enveloped RNA viruses and various light conditions, e.g. UVC, UVA and indoor light. Doss et al. [14] reported the inactivation of bacteriophage T2 using TiO_2/beta SiC foams exposed by UVA emitting LEDs with an emission maximum at 392 nm. The used system exhibited a filtration effect achieved by the presence of SiC foam and also an effect of photocatalytic inactivation. With 56 LEDs the effect of inactivation was about 3 logs for 60 minutes of runtime. The pure filtration effect in the dark resulted in a decay of 1 log. Lee et al. [15] investigated the inactivation of the murine norovirus (MNV) as a surrogate for the human norovirus using both a plaque assay and a real-time TaqMan reverse transcription (RT)-PCR assay. The amount of MNV was significantly reduced by 254 nm UVC light and the presence of TiO_2 had a minor effect. Khaiboullina et al. [16] evaluated the virucidal efficacy (using HCoV-NL63, a close genetic relative of SARS-CoV-2) of photoactive TiO_2 nanoparticles deposited on glass coverslips and UVC light (256 nm, irradiation intensity ranged from 2.9 to

13 mW cm^{-2}) by RT-qPCR and virus infectivity assays. Using RT-qPCR, which serves to quantify viral RNA, it was found that due to UVC light alone, there is a decrease in viral copies by RT-qPCR from 150 to about 20 after 0.5 min and to 10 after 1 min. Due to UVC light in combination with TiO_2, there is a decrease in viral copies by RT-qPCR from 150 to about 3 after 0.5 min and to zero after 1 min.

Nakano et al. [17] demonstrated the inactivation of the influenza virus through TiO_2 photocatalysis using TiO_2 nanoparticles immobilized on a glass plate. The photocatalytic reaction was performed according to ISO27447:2009(E) [18] and JIS R 1702 [19] (antibacterial efficiency) with minor modifications. The viral titres were dramatically reduced by the photocatalytic reaction. Even with a low intensity of UVA (0.01 mW cm^{-2}), a viral reduction of approximately 4-log_{10} was observed within a short irradiation time. The viral inactivation kinetics were associated with the exposure time, the UV intensity and the BSA concentration in virus suspensions. These results show that TiO_2 photocatalysis could be used to inactivate the influenza virus. Furthermore, a minor modification of the ISO test method for anti-bacterial effects of TiO_2 photocatalysis could be useful for the evaluation of antiviral activity.

Yoshizava et al. [20] investigated the virucidal effect of photocatalytic material using Bovine Coronavirus (BCoV) as a model of pathogenic SARS-CoV-2 and SARS-CoV-1. The testing procedure was realised using ISO 18071 [21] facilitating the assessment of the antiviral activity of the photocatalytic material (a mixture of a peroxotitanium acid solution (70%) and a peroxo-modified anatase solution (30%)) under the indoor light environment.

The recent pandemic showed us that there is a strong demand for standardized methods to evaluate the antiviral activity of different materials using enveloped RNA viruses (e.g. SARS-CoV-2, influenza virus). Although several standardized methods evaluating antiviral activity on different surfaces in the dark use the influenza virus [22], [23], all standardized methods evaluating the antiviral activity of photocatalytic surfaces use bacteriophage Q-beta, a representative of small non-enveloped viruses [21], [24], [25]. The aim of this work is therefore to evaluate the virucidal efficiency of photocatalytically active nanostructured TiO_2 surfaces (including 1D nanotubular layers) in inactivation a model "enveloped RNA virus" – the influenza virus (influenza A H1N1 California). Particular interest is given to the methodology of virucidal testing and the influence of the surface nanostructure (porosity) on the determined virucidal efficiency.

2. Experimental

2.1 *Preparation and characterization of surfaces used for virucidal testing*

i) Composite TiO_2/SiO_2 layers (sample C) contain particles of the photocatalyst Aeroxide P25 (TiO_2) dispersed in a binder system based on tetraethoxysilane TEOS and colloidal SiO_2, details of the preparation were reported previously [26]. Soda lime glass was used as a substrate (25 × 75 × 1 mm and 20 × 20 × 1 mm).

ii) Sol-gel TiO_2 layers (sample S) were deposited by dip-coating using the sol-gel method based on Ti-isopropoxide [27]. To prevent the diffusion of Na^+ ions from the soda-lime glass substrate during calcination, the layers were applied on FTO glass substrates (25 × 75 × 1 mm and 20 × 20 × 1 mm) where the conductive SnO_2 layer serves as a protective barrier.

iii) Nanotubular layers (samples TNT5 and TNT7) were prepared by anodic oxidation of Ti foil. The electrolyte used consisted of ethylene glycol containing 150 mM NH_4F and 10 vol.% H_2O. The anodization was carried out at 80 V for 4 h [11]. Different nanotube layer thicknesses were achieved by using electrolytes of different age (i.e. being used for different times before the final anodization to prepare the nanotube layers) [28]. This means that the ~7 µm thick TNT layers were prepared in a fresh electrolyte which was used once before for TNT layer preparation, while the ~5 µm thick TNT layers were prepared in an electrolyte which was used 7 times before to produce TNT layers. The reason for this is that the electrolyte composition is changing with its use as the concentration of F^- ions decreases due to the formation of the $[TiF_6]^{2-}$ complex and the H_2O content increases due to electrode reactions. Electrolytes which were used several times are therefore weaker, resulting in thinner TNT layers.

All types of tested surfaces were first characterised (thickness, morphology, photocatalytic activity). The layer thickness of samples C, and S was determined using the DektaXT profilometer (Bruker). The nanotube layer thicknesses (samples TNT5 and TNT7) and surface morphologies of all samples were determined by scanning electron SEM, Hitachi S4800).

2.2. *Measurement of photocatalytic activity*

The photocatalytic activity was evaluated using the herbicide monuron as a model compound representing a non-polar pollutant [29, 30]. A magnetically stirred batch-mode water-cooled photoreactor was used [31]. The volume of aqueous pollutants was 25 cm^3. The

photocatalyst layers were irradiated by UV light (Sylvania Lynx CFS 11 W BL350 fluorescent UV light tubes) with a spectral maximum at 365 nm. The intensity of incident light on the surface of the photocatalysts was 1.9 mW cm^{-2}. The irradiated area was 10 cm^2. The initial concentration and pH of monuron were $1 \cdot 10^{-4}$ mol dm^{-3} and 5.7, respectively. Monuron has an absorption maximum in the UV region at a wavelength of 244 nm ($\varepsilon = 1.73 \cdot 10^4$ dm^3 mol^{-1} cm^{-1}) and does not absorb above 300 nm. The concentration of monuron was followed by HPLC analysis, employing a Shimadzu modular system Nexera lite with a photodiode array detector SPD-M40. As mobile phase methanol/water (60:40, v/v) was applied, with a flow rate of 1 ml min^{-1} and a LiChrospher 100 RP-18 column (type LiChroCART 125-4, Merck, Germany). The concentration of the pollutant was followed as a function of irradiation time. The photocatalytic activities were compared via apparent first-order rate constant (k, min^{-1}) and initial degradation rate (r_i, nmol cm^{-2} min^{-1}), calculated from the slope of the concentration decay during first 60 min of irradiation, as described elsewhere [31].

2.3. Evaluation of virucidal efficiency using RNA virus

The virucidal efficacy of photocatalytically active surfaces was evaluated using a representative of enveloped RNA viruses – the influenza virus. The methodology is based on the standard method of determining the virucidal effect of photocatalytically active surfaces using the Q-beta bacteriophage as a representative of a small non-enveloped virus (ISO 18061:2014) [24]. It is based on a comparison of virus infectivity on the active irradiated surface, the active non-irradiated surface, the control irradiated surface and the control non-irradiated surface.

AUV lamp (365 nm, intensity 0.25 mW cm^{-2}) was used for the tests. The tested samples of photocatalytically active layers (marked "S", "C", "TNT5" and "TNT7") were prepared in the form of squares of 20 × 20 mm. The virucidal effect of photocatalytically active layers was tested by applying the influenza virus (Influenza A H1N1/California/07/2009, Diagnostic Hybrids, Athens, OH, United States). The influenza virus was propagated in MDCK (defined in detail in SI) cells (ATCC CCL-34) cultured in influenza growth medium (IGM), which consists of DMEM supplemented with Pen/Strep, 0.2% BSA, 1 mM HEPES, 13.6 mM L-glutamine, 42 µg mL^{-1} DEAE-Dextran, 1 µg mL^{-1} TPCK-Trypsine). The tested samples were placed in a Petri dish, 50 µL of virus suspension (50% tissue culture infectious dose, TCID50 ~ 6×10^6 PFU mL^{-1}) was applied to the surface of the active layer. The same virus applied to a control glass without an active layer was used as a control. The virucidal effect was measured

after 2 hours of exposure, both under and without UV light. The virus was then washed out with 450 µL IGM and the influenza virus titre was determined by using a 10-fold serial dilution with IGM. The rest of the samples were used for viral RNA extraction. MDCK cells were seeded on the 24-well plate a day before the experiment (250.10^3 cells/1 mL DMEM/10%FBS/PENSTREP). On the day of the experiment, the cells were washed once with PBS, 300 µL of recovered virus was added to the cells, and incubated for 1 h at 37 °C / 5% CO_2. After 1 h, the cells were washed once with PBS, 300 µL of IGM was added to the cells and the medium was overlaid with 300 µL of 1.2% carboxymethyl cellulose, and incubated for 2 days at 37 °C / 5% CO_2. The infectious virus was detected using a plaque assay. The infection was terminated by aspirating the medium. Cells were washed once with PBS and fixed and stained with naphthalene black. After 45 min of incubation, the naphthalene black solution was aspirated, cells were washed with water and the resulting plaques were counted and the viral titre was expressed in PFU/mL. Three biological replicates were used to generate all of the data.

2.4. Evaluation of the RNA virus retained in the inner space of nanostructures

Virus washouts were used to quantify the influenza virus RNA levels. RNA was extracted using QIAamp Viral RNA Mini Kit (Qiagen, Maryland, USA) from each sample used for influenza virus TCID50 measurement. On each sample also a 2nd wash step was applied to examine the efficacy of the 1st wash from the surfaces. The 2nd virus washouts were prepared by putting each sample into a Petri dish with 2 mL PBS under horizontal agitating (440 rpm) for 12 hours.

3. Results

3.1 Morphology characterization of photocatalytic surfaces

Fig. 1 shows SEM images demonstrating the morphology of the individual TiO_2 layers, composite (C), sol-gel (S) and nanotubular (TNT). In the case of sample C, the open porous structure of the surface is noticeable. The surface of sample S has is rather smooth, small particles (20-30 nm) are visible. The nanotube layers (TNT5 and TNT7) consist of nanotubes with an internal diameter of ~180 nm (i.e. 179.7 ± 19.7 nm and 176.0 ± 24.9 nm for the ~5 µm and ~7 µm thick TNT layers, respectively) and a wall thickness of ~15 nm (i.e. 15.7 ± 3.1 nm and 14.8 ± 3.0 nm for the ~5 µm and ~7 µm thick TNT layers, respectively).

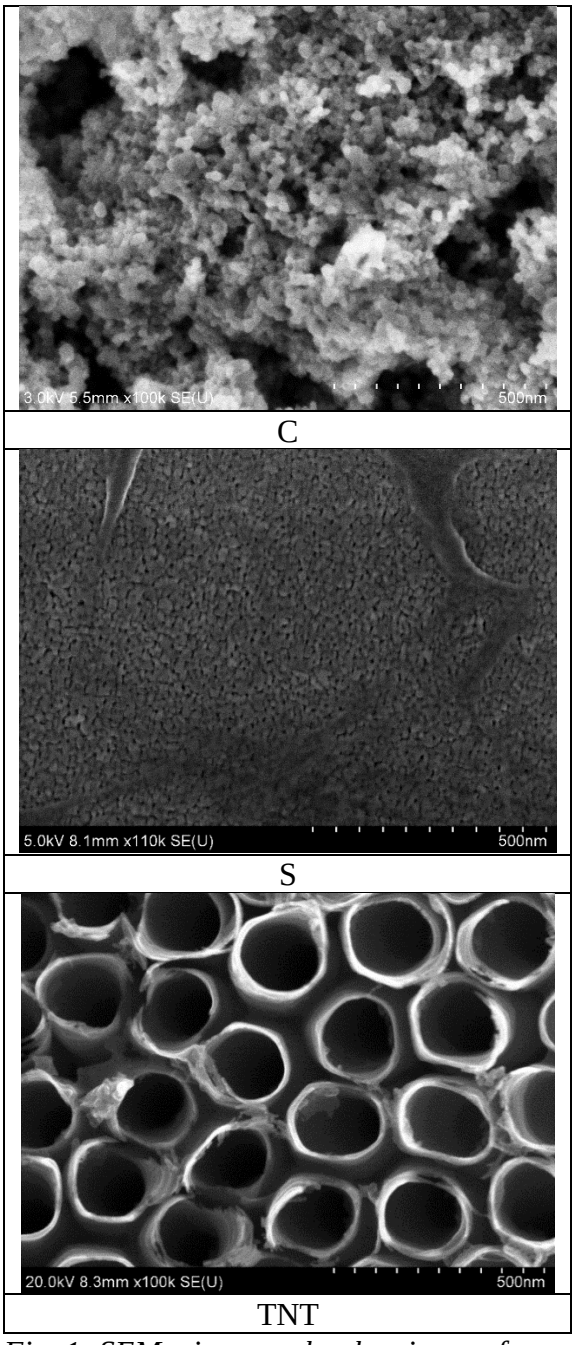

Fig. 1: SEM micrographs showing surface morphologies of the tested samples.

Table 1 summarises all types of tested photocatalytic TiO_2 surfaces.

Table 1: Summary of photocatalytic TiO_2 surfaces used for testing.

Type of sample	Name	Description	Layer thickness (µm)	Porosity (%)
Composite TiO_2/SiO_2 on glass	**C**	high porosity	5	74*
sol gel TiO_2 on glass	**S**	low porosity	0.1	4**

Nanotubular TiO_2 on Ti foil	**TNT5**	TNT diameter 180 nm	5	70***
	TNT7	TNT diameter 180 nm	7	70***

* Calculated according to eq. (1) using average density of composite TiO_2/SiO_2 coating (3.3 g cm^{-3}).
** Calculated according to eq (1) using a density of TiO_2 (3.8 g cm^{-3}) in our previous work [32].
*** Calculated according to eq (2) [33], [34],

$$P = \frac{V_{air}}{V_{layer}} 100 = \frac{V_{layer} - V_{TiO2}}{V_{layer}} 100 = \frac{(h - \frac{m_{layer}}{1000.S.\rho_{TiO2}})}{h} 100 \quad (1)$$

$$P = 1 - \frac{2\pi w(w + d_{in})}{\sqrt{3}(d_{in} + 2w)^2} \quad (2)$$

where V is the volume, m is the mass, ρ is the denisty, w is the nanotube wall thickness and d_{in} the inner diameter of the nanotubes.

It must be noted that the calculated porosity values are estimations and not accurately measured values.

3.2 Photocatalytic activity – oxidative removal of model organic pollutant

Fig. 2 shows the concentration decay of the model herbicide monuron during the photocatalytic degradation experiments using the different catalysts in a batch photoreactor. From the concentration dependence in the first 60 minutes, the initial degradation rate, r_i (mol min cm^{-2}), was calculated according to the formula:

$$r_i = \frac{V}{S}\left(\frac{dc}{dt}\right)_{60} \quad (3)$$

where $(dc/dt)_{60}$ is the slope of the concentration dependence during the initial 60 minutes, V is the volume of the photoreactor in dm^3 a S is the irradiated area in cm^2.

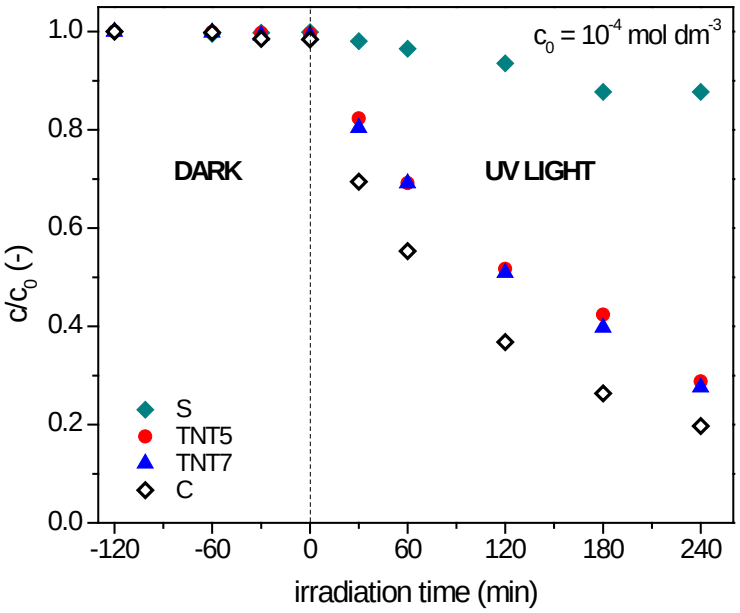

Fig.2: A decay of the monuron concentration during the photocatalytic experiment.

Table 2 summarises the photocatalytic activity of the tested TiO_2 photocatalytic surfaces, e.g. values of r_i and apparent first order constant k. The highest photocatalytic activity was observed for the composite layer consisting of TiO_2 particles and SiO_2 binder (sample C), the lowest activity for sample S. Samples TNT5 and TNT7 achieved about 65 % of the activity of sample C. Ten times lower photocatalytic activity of the sample S in comparison with the sample C can be explained by a significantly lower thickness (50 times) and reduced surface area due to low porosity. However, it is worth to note that all samples were photocatalytically active.

Table 2. Summary of photocatalytic activity of tested surfaces

Type of sample	Name	Description	Initial rate of photocatalytic degradation, r_i (mol min^{-1} cm^{-2})	k (min^{-1})
Composite TiO_2 /SiO_2 on glass	**C**	thickness 5 μm, high porosity	21.4×10^{-8}	6.5×10^{-3}
Sol gel TiO_2 on glass	**S**	thickness 100 nm, low porosity	1.4×10^{-8}	0.6×10^{-3}
Nanotubular TiO_2 on Ti foil	**TNT5**	thickness 5μm, diameter 180 nm	13.8×10^{-8}	4.9×10^{-3}
	TNT7	thickness 7μm, diameter 180 nm	13.7×10^{-8}	5.1×10^{-3}

3.3 Photocatalytic activity – inactivation of RNA virus

3.3.1 Validity requirements, stability of viruses in the dark

To ensure the robustness of the proposed method, titres of infectious virus in the inoculum are always verified during individual experiments. This will avoid cases, where there would be a significant inactivation of the virus unrelated to the course of the experiment and the conditions, to which the inoculum is exposed during the experiment. The validity requirements are defined in detail in SI.

Due to the possible problem of non-reproducibility of the analytical determination of the virus amount on the control surface (glass), the amount of the influenza virus on the control surface (glass) was first determined during exposure in the dark. Typical experimental results are shown in Table S1 (in SI). After 2 hours in the dark, the amount of analytically determined virus on the control surface decreased by 41 % (0.2 log).

3.3.2. Determination of virucidal efficiency

According to ISO 18061:2014, the resulting virucidal activity (α-bacteriophage) of the surface (ΔV) is given by equations (4) and (5):

$$V_L = \log\left(\frac{B_L}{A}\right) - \log\left(\frac{C_L}{A}\right) = \log\left(\frac{B_L}{C_L}\right) \quad (4)$$

$$\Delta V = \log\left(\frac{B_L}{C_L}\right) - [\log\left(\frac{B_D}{A}\right) - \log\left(\frac{C_D}{A}\right)] = \log\left(\frac{B_L}{C_L}\right) - \log\left(\frac{B_D}{C_D}\right) \quad (5)$$

where

V_L is the virucidal activity of the surface after UVA irradiation of intensity (mW cm^{-2})

ΔV is the virucidal activity of the surface caused by UVA irradiation

A is the average virus titre on the control surface immediately after inoculation (time 0)

B_L is the virus titre on the control surface under UVA irradiation (2 h)

C_L is the virus titre on the photocatalytically active surface under UVA irradiation (2 h)

B_D is the virus titre on the control surface in the dark (2 h)

C_D is the virus titre on a photocatalytically active surface in the dark (2 h).

Experiments evaluating virucidal effects have shown that the A value on the control surface (B) and the photocatalytically active surface (C) differed. It is therefore more accurate in the calculation ΔV to use both values of A:

$$V_L = \log\left(\frac{B_L}{A_B}\right) - \log\left(\frac{C_L}{A_C}\right) \quad (6)$$

$$\Delta V = \left[\log\left(\frac{B_L}{A_B}\right) - \log\left(\frac{C_L}{A_C}\right)\right] - [\log\left(\frac{B_D}{A_B}\right) - \log\left(\frac{C_D}{A_C}\right)] = V_L - V_D \quad (7)$$

where

A_B is the virus titre on the control surface immediately after application of the virus suspension (time 0),

A_C is the virus titre on the photocatalytically active surface immediately after application of the virus suspension (time 0), and

V_D is the apparent virucidal activity of a photocatalytically active surface in the dark.

Virus titre and recovery

A virus titre was determined for each test of the virucidal effect of the photocatalytic active layer. The average value of the virus titre (TCID50) was then used to calculate the so-called **recovery of the control surface**, **Rec(B)**, i.e. the **ratio** of the virus titre determined immediately after the virus is applied to the control surface and subsequent rinsing and the virus titre that is applied to the surface, and the recovery of the photocatalytic active surface, **Rec(C)**, i.e. the

ratio of the virus titre determined immediately after the virus is applied to the photocatalytically active surface and subsequent rinsing and titre of the virus, which is applied to the surface.

$$Rec(B)(\%) = 100\left(\frac{A_B}{TCID50}\right) \quad (8)$$

$$Rec(C)(\%) = 100\left(\frac{A_C}{TCID50}\right) \quad (9)$$

The calculated recovery values **Rec(B)** and **Rec(C)** are compared in Table S2 (in SA). Recovery values fluctuate for both the control and active sample, but the absolute difference between the control and active samples is always small (from 1 to 21 % which corresponds to a maximum difference of 0.13 log).

The mean values of A_B, A_C, B_L, C_L, B_D, C_D together with the values of V_L, V_D and ΔV calculated according to equations (6) and (7), which express how virucidal the surface is, are shown in Table 3 for the **influenza** virus and the photocatalytically active sample TNT5. Data for the other three samples are shown in the SI (Table S3, S4 and S5).

Table 3. Evaluation of virucidal efficiency (influenza virus) of sample TNT5, 2 h exposition.

sample: TNT5	PFU/cm2	log PFU/cm2		Average PFU/cm2	Average log PFU/cm2	Error log PFU/cm2		
virus titre	1.800E+06	6.255	TCID50	2144444	6.33	0.07		
	2.167E+06	6.336						
	2.467E+06	6.392						
sample (time 0h)	1.600E+06	6.204	A_C	1477777	6.16	0.08	**69**	**Rec(C) %**
	1.167E+06	6.067						
	1.667E+06	6.222						
control, (time 0h)	1.600E+06	6.204	A_B	1677777	6.22	0.06	**78**	**Rec(B) %**
	1.933E+06	6.286						
	1.500E+06	6.176						
sample, light (time 2h)	3.333E+02	2.523	C_L	444	2.62	0.17	**2.07**	**V_L**
	6.667E+02	2.824						
	3.333E+02	2.523						
control, light (time 2h)	7.333E+04	4.865	B_L	58889	4.76	0.10		
	5.667E+04	4.753						
	4.667E+04	4.669						
sample dark (time 2h)	9.333E+04	4.970	C_D	106667	5.03	0.05	**0.92**	**V_D**
	1.167E+05	5.067						
	1.100E+05	5.041						
control, dark (time 2h)	1.233E+06	6.091	B_D	1000000	5.99	0.09		
	8.333E+05	5.921						
	9.333E+05	5.970						
							1.15	**ΔV**

V_D, V_L a ΔV calculated using equations (6) and (7) are compared in Table 4 for all tested samples. Since TiO_2 itself has no virucidal effect in the dark, it is evident that the virus is

retained on the surface of the active samples during exposure in the dark. As a result, there was a significant decrease in the amount of viral RNA and also in viral titer, obtained after the rinsing after the exposure in the dark. This decrease, expressed as V_D, can therefore be understood as an additional effect of virus retention in pores of nanostructure, which was already shown by Hosseini et al. [35]. It turned out that the virus retention is higher for the porous surface (sample C), while it is lower for the sample with very low porosity (sample S). In the case of a special surface, which is a surface consisting of regular nanotubes (samples TNT5 and TNT7), the virus retention is between the values for the two surfaces (C and S). However, it should be emphasized that this fact is taken into account in the calculation of virucidal efficacy. In addition, the calculation of virucidal efficacy ΔV is refined by including A_B (A_C), which is the virus titre on the control (photocatalytically active) surface immediately after application of the virus suspension (time 0). It should be emphasized that although sample C showed an order of magnitude higher photocatalytic activity than sample S (see Fig. 2), the values of ΔV are for both samples comparable, in fact for sample S it is higher.

Table 4. Comparison of virucidal efficiency of TiO_2 surfaces.

Sample name	TiO_2 layer	Influenza A		
		V_L	V_D	ΔV
C	high porosity, 5 µm,	1.85	1.81	0.05
S	low porosity, 100 nm,	0.64	0	0.66
TNT5	Nanotubular, thickness 5µm, diameter 180 nm	2.07	0.92	1.15
TNT7	Nanotubular, thickness 7µm, diameter 180 nm	2.78	1.23	1.56

3.3.3 Evaluation of RNA virus retained in the inner space of nanostructures

Recovered influenza viral genome copies were determined by reverse-transcription quantitative PCR (RT-qPCR). The virus retention in the nanostructures of the tested surfaces was evaluated in comparison with non-porous control glass. Surfaces of samples with high porosity (C, TNT5 and TNT7) have the capability to retain the influenza virus in contrast to sample S with low porosity and the control glass with a non-porous surface (Fig 3a). The RNA amount immediately washed from samples (time „0“) was almost the same for all surfaces. The same relative amount of RNA was also detected in control samples after 2-hour incubation. In

contrast, after 2 hours of incubation, no matter if with or without UV illumination, the RNA amount was unambiguous lower in washes from samples containing nanostructures of high porosity (samples C, TNT5 and TNT7). All these observations are also demonstrated on raw data of Ct values in Fig. 3b.

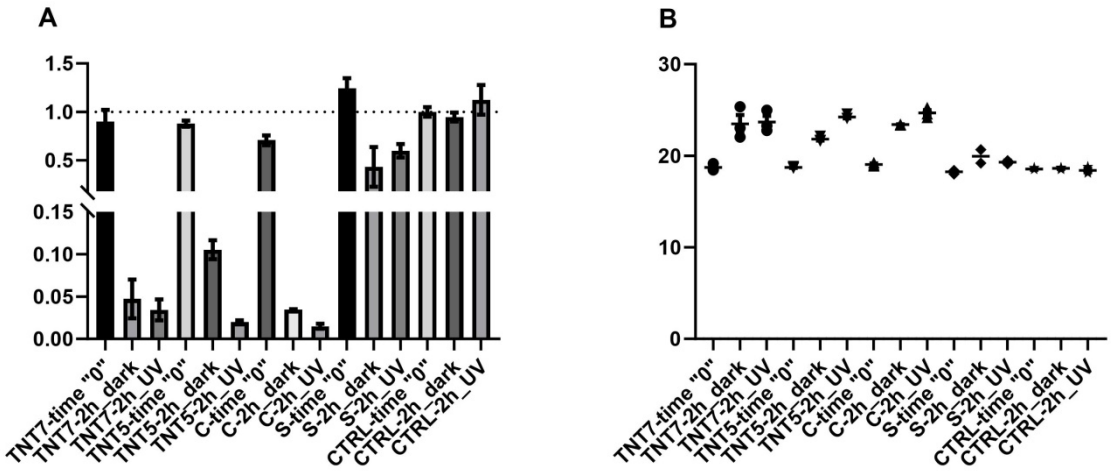

Fig. 3. A) Relative RNA amount from the wash used for infection (1st wash), data are plotted as a fold change of each sample related to the control at the time „0“. B) raw Ct values from RT-qPCR of RNA from (1st wash).

The decrease of the virus TCID50 may correlate with the reduction of genome copies, however, it was shown, that the genome copy reduction may not be as fast, as the decrease in infectivity [36]. The relation of viral infectivity (represented by TCID50 value) and recovered viral genome copies (RT-qPCR) are shown in Fig. 4. There were no big differences in the amount of recovered residual virus measured by its infectivity or relative level of RNA at the time „0“ for all of the tested surfaces, including the control glass. The situation was changed after 2-hour exposition in the dark. There was an evident drop in the relative amount of residual virus for surfaces TNT7, TNT5 and C in comparison with sample S and the control sample for both methods of measurement. This is given by the ability of porous materials to draw droplets containing virions into their nanostructures. In the case of 2 h expositions with UV irradiation, another decrease of the relative amount of residual virus may be caused by the real antiviral effect given by the activated TiO_2 for samples with an active surface. TCID50 decrease of control sample after 2 h with UV irradiation is a natural effect of own virus inactivation under

the experimental conditions. Based on these data, we can summarize that surface porosity plays a significant role in viral persistence as was shown previously [35, 37].

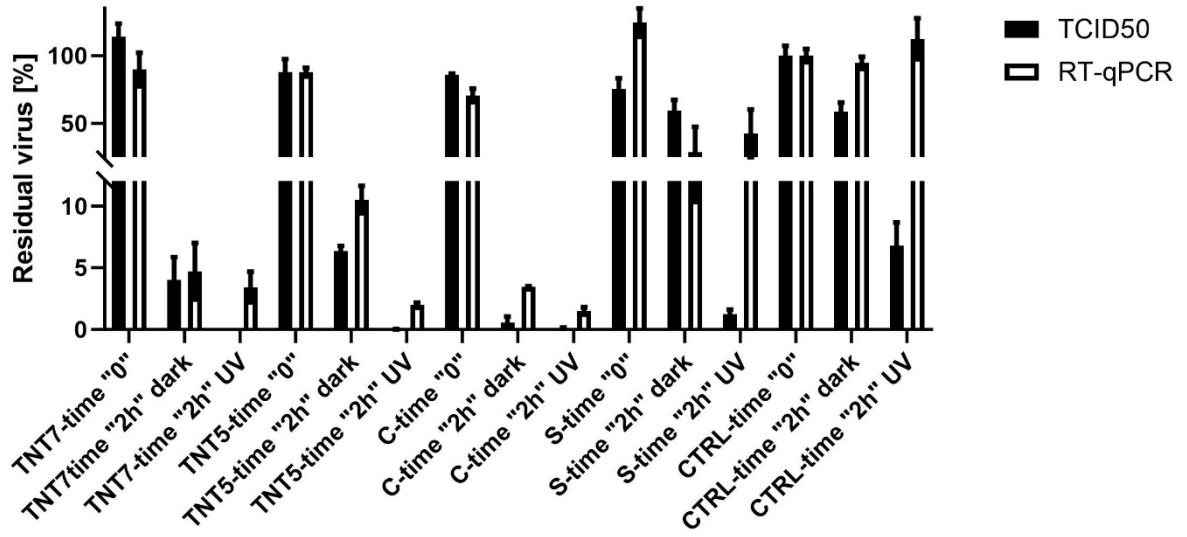

Figure 4. Comparison of infectivity of recovered virus (TCID50) and RNA amount (RT-qPCR). Data are plotted as a percentage of each sample related to the control at the time „0".

Fig. 5 shows the relative amount of RNA washed from the tested samples and raw Ct values in the 2nd wash solutions. The 2nd wash was applied to find out, how much RNA remained on the surface after the first wash and if there was any difference in the RNA level in the second wash between porous surfaces of high porosity (C, TNT5 and TNT7) and surfaces of no or low porosity (CTRL, S). For the low porosity or non-porous surfaces, the amount of RNA in the 2nd wash was approximately 280 times (S) or 270 times lower (CTRL) than the amount of RNA in the 1st wash. This indicates that only about 0.4 % of the influenza virus was not washed out during the 1st wash. On the other hand, the results in Fig. 5a show, that from the porous surfaces, it was washed in average 170× (surface TNT7), 145× (surface TNT5) and 25× (surface C) less RNA in comparison with non-porous materials. All these observations are also demonstrated on raw data of Ct values in Fig. 5b. This means that the relative amount of RNA in the 2nd wash was obviously less from the porous surfaces in comparison with surfaces of low porosity (S, CTRL).

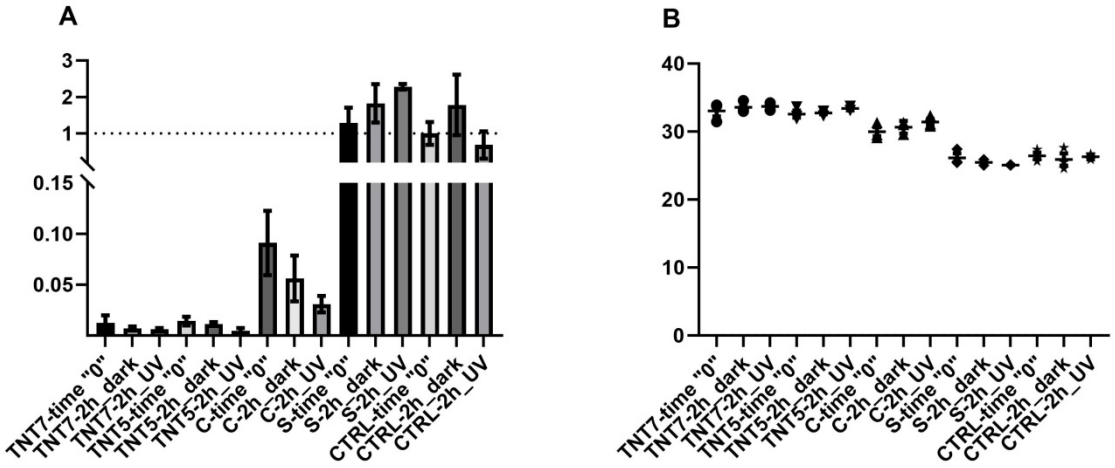

Fig. 5. A) Relative RNA amount washed from the tested samples (2nd wash), data are plotted as a fold change of each sample related to the control at the time „0“. B) raw Ct values from RT-qPCR of RNA from (2nd wash).

It can be concluded that the amount of washed RNA correlates with the nanostructural complexity of the tested surfaces. In contrast to the Ct data from the 1st first wash, where the 2-hour sample incubation leads to the RNA level decrease in nanostructural surfaces (Fig. 3b), the Ct values from the second wash (Fig. 5b) contained relative RNA level approximately the same for all treatments (0, 2 h dark, 2 h UV). Differences were observed only between surfaces.

4. Conclusions

Two types of nanostructured (nanotubular and nanoparticle) TiO_2 coatings of high porosity were fabricated and their photocatalytic activity (to oxidatively remove aqueous pollutants) and virucidal activity under UV light (enveloped RNA virus - influenza virus) were evaluated and compared with that of low porosity TiO_2 coating. The virucidal efficacy of photocatalytically active nanoparticles and nanotubular surfaces was successfully evaluated using a representative of enveloped RNA viruses – influenza virus. The methodology was based on the standard method of determining the virucidal effect of photocatalytically active surfaces using the Q-beta bacteriophage as a representative of a small non-enveloped virus (ISO 18061:2014).

The virucidal tests were affected by the fact that the virus is retained on the surface of the nanostructured TiO_2 during exposure in the dark. As a result, there was a significant decrease

in the amount of viral RNA and also in viral titer, obtained after the rinsing. This decrease can be understood as an additional effect of virus retention in pores of the nanostructure. The virus retention is higher for the porous surface, while for surfaces with very low porosity, it is lower. However, it should be emphasized that this fact is taken into account in the calculation of virucidal activity due to UV light.

Both nanostructured TiO_2 coatings have comparable porosity and thickness but photocatalytic activity is higher for nanoparticles than for nanotubular surfaces. On the other hand, the virucidal activity is much higher for nanotubular surfaces. It should be emphasized that although a high porosity surface showed an order of magnitude higher photocatalytic activity than a low porosity surface, the values of virucidal activity are comparable for both surfaces, in fact for low porosity surfaces it is higher.

Acknowledgement

The authors acknowledge the Czech Science Foundation (project 21-27243S) and the Ministry of Education, Youth and Sports of the Czech Republic (MEYS CR, project LM2023037). This work was also supported by Specific university research grant – No A1_FCHT_2023_004. Experiments with influenza were supported by VES19IZRAEL INTER-EXCELLENCE, subprogram INTER-ACTION LTAIZ19017 from MEYS CR.

5. References

1. B, A.H., M. Azab El-Liethy, and G.E. El-Taweel, *The destruction of Escherichia coli adhered to pipe surfaces in a model drinking water distribution system via various antibiofilm agents.* Water Environ Res, 2020. **92**(12): p. 2155-2167.
2. Bai, X.Q., et al., *Study on biomimetic preparation of shell surface microstructure for ship antifouling.* Wear, 2013. **306**(1): p. 285-295.
3. Xie, F., et al., *Versatile antibacterial surface with amphiphilic quaternized chitin-based derivatives for catheter associated infection prevention.* Carbohydrate Polymers, 2022. **275**: p. 118683.
4. Li, X., et al., *Recent developments in smart antibacterial surfaces to inhibit biofilm formation and bacterial infections.* Journal of Materials Chemistry B, 2018. **6**(26): p. 4274-4292.
5. Dallas, P., V.K. Sharma, and R. Zboril, *Silver polymeric nanocomposites as advanced antimicrobial agents: Classification, synthetic paths, applications, and perspectives.* Advances in Colloid and Interface Science, 2011. **166**(1-2): p. 119-135.
6. Slamborova, I., et al., *New type of protective hybrid and nanocomposite hybrid coatings containing silver and copper with an excellent antibacterial effect especially against MRSA.* Materials Science & Engineering C-Materials for Biological Applications, 2013. **33**(1): p. 265-273.
7. Elechiguerra, J.L., et al., *Interaction of silver nanoparticles with HIV-1.* Journal of Nanobiotechnology, 2005. **3**(1): p. 6.
8. Hodek, J., et al., *Protective hybrid coating containing silver, copper and zinc cations effective against human immunodeficiency virus and other enveloped viruses.* Bmc Microbiology, 2016. **16**: p. 12.
9. Macak, J.M., et al., *TiO2 nanotubes: Self-organized electrochemical formation, properties and applications.* Current Opinion in Solid State and Materials Science, 2007. **11**(1): p. 3-18.
10. Lee, K., A. Mazare, and P. Schmuki, *One-Dimensional Titanium Dioxide Nanomaterials: Nanotubes.* Chemical Reviews, 2014. **114**(19): p. 9385-9454.
11. Sopha, H., et al., *Scaling up anodic TiO2 nanotube layers – Influence of the nanotube layer thickness on the photocatalytic degradation of hexane and benzene.* Applied Materials Today, 2022. **29**.
12. Macak, J.M., H. Tsuchiya, and P. Schmuki, Angew. Chem., Int. Ed., 2005. **44**: p. 2100.
13. Macak, J.M., et al., *Self-Organized TiO2 Nanotube Layers as Highly Efficient Photocatalysts.* Small, 2007. **3**(2): p. 300-304.
14. Doss, N., et al., *Photocatalytic Decontamination of Airborne T2 Bacteriophage Viruses in a Small-Size TiO2/β-SiC Alveolar Foam LED Reactor.* Water, Air, & Soil Pollution, 2018. **229**(2): p. 29.
15. Lee, J., K.D. Zoh, and G. Ko, *Inactivation and UV disinfection of murine norovirus with TiO2 under various environmental conditions.* Applied and Environmental Microbiology, 2008. **74**(7): p. 2111-2117.
16. Khaiboullina, S., et al., *Inactivation of Human Coronavirus by Titania Nanoparticle Coatings and UVC Radiation: Throwing Light on SARS-CoV-2.* Viruses, 2021. **13**(1): p. 19.
17. Nakano, R., et al., *Photocatalytic inactivation of influenza virus by titanium dioxide thin film.* Photochemical & Photobiological Sciences, 2012. **11**(8): p. 1293-1298.
18. *ISO 27447:2009(E), Fine ceramics (advanced ceramics, advanced technical ceramics) – Test method for antibacterial activity of semiconducting photocatalytic materials, 2009.*
19. *JIS R 1702, Fine ceramics (advanced ceramics, advanced technical ceramics) – Test method for antibacterial activity of photocatalytic products under photoirradiation and efficacy, 2006.*
20. Yoshizawa, N., et al. *Application of a Photocatalyst as an Inactivator of Bovine Coronavirus*. Viruses, 2020. **12**, DOI: 10.3390/v12121372.
21. *ISO 18071:2016 Fine ceramics (advanced ceramics, advanced technical ceramics) - Determination of antiviral activity of semiconducting photocatalytic materials under indoor lighting environment - Test method using bacteriophage Q-beta*. 2016.
22. *ISO 18184: 2019 Textiles - Determination of antiviral activity of textile products*. 2019: Geneva.
23. *ISO 21702:2019 Measurement of antiviral activity on plastics and other non-porous surfaces*. 2019: Geneva.
24. *ISO 18061:2019 Fine Ceramics (advanced ceramics, advanced technical ceramics) - Determination of antiviral activity of semiconducting photocatalytic materials — Test method using bacteriophage Q-beta*. 2019: Geneva.
25. *JIS R 1706, Revision 20J, January 20, 2020 - Fine ceramics (advanced ceramics, advanced technical ceramics) - Determination of antiviral activity of photocatalytic materials - Test method using bacteriophage Q-beta.* 2020.

26. Rusek, J., et al., *Composite TiO2 films modified by CeO2 and SiO2 for the photocatalytic removal of water pollutants.* Photochemical & Photobiological Sciences, 2022.
27. Krýsa, J., M. Baudys, and A. Mills, *Quantum yield measurements for the photocatalytic oxidation of Acid Orange 7 (AO7) and reduction of 2,6-dichlorindophenol (DCIP) on transparent TiO2 films of various thickness.* Catalysis Today, 2015. **240**: p. 132-137.
28. Sopha, H., et al., *Effect of electrolyte age and potential changes on the morphology of TiO2 nanotubes.* Journal of Electroanalytical Chemistry, 2015. **759**: p. 122-128.
29. Rusek, J., et al., *Composite TiO2-SiO2-REOs photocatalysts for water treatment: Degradation kinetics of monuron and its intermediates.* Journal of Photochemistry and Photobiology A: Chemistry, 2023. **445**.
30. Krýsa, J., et al., *Photocatalytic degradation of model organic pollutants on an immobilized particulate TiO2 layer. Roles of adsorption processes and mechanistic complexity.* Applied Catalysis B: Environmental, 2006. **64**(3-4): p. 290-301.
31. Krýsa, J., et al., *Photoactivity assessment of TiO 2 thin films using acid Orange 7 and 4-chlorophenol as model compounds. Part I: Key dependencies.* Journal of Photochemistry and Photobiology A: Chemistry, 2012. **250**: p. 66-71.
32. Zita, J., et al., *Photocatalytic properties of different TiO2 thin films of various porosity and titania loading.* Catalysis Today, 2011. **161**(1): p. 29-34.
33. Zhu, K., et al., *Enhanced Charge-Collection Efficiencies and Light Scattering in Dye-Sensitized Solar Cells Using Oriented TiO2 Nanotubes Arrays.* Nano Letters, 2007. **7**(1): p. 69-74.
34. Sopha, H., et al., *Scaling up anodic TiO2 nanotube layers – Influence of the nanotube layer thickness on the photocatalytic degradation of hexane and benzene.* Applied Materials Today, 2022. **29**: p. 101567.
35. Hosseini, M., et al., *Effect of Surface Porosity on SARS-CoV-2 Fomite Infectivity.* Acs Omega, 2022. **7**(22): p. 18238-18246.
36. Obrova, K., et al., *Decontamination of High-Efficiency Mask Filters From Respiratory Pathogens Including SARS-CoV-2 by Non-thermal Plasma.* Frontiers in Bioengineering and Biotechnology, 2022. **10**: p. 13.
37. Owen, L., et al., *Porous surfaces: stability and recovery of coronaviruses.* Interface Focus, 2021. **12**(1): p. 12.